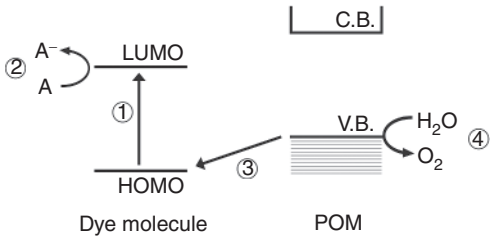

Figure 1.12 Electron transfer processes in a dye-sensitized O_2 evolution system. C.B., conduction band; V.B., valence band; HOMO, highest occupied molecular orbital; LUMO, lowest unoccupied molecular orbital; A, electron acceptor; A^-, reduced electron acceptor.

The light-absorption property of POMs can be controlled by manipulating their metal cations and their cluster sizes, and such adjustability is useful for achieving a basic understanding of their properties [79].

Exploiting the unique character of POMs enables the effect of the number of active sites to be studied, which is necessary to facilitate the surface catalytic reactions. To reveal the effect of the number of active sites, the effect of the cluster size on the DSP reaction was investigated using three molecular molybdenum-oxo materials with different sizes but with the same triclinic space group and similar light-absorption properties [80]. This system was used for DSP of the O_2-evolution reaction. The reaction flow differs from that in the H_2-evolution reaction discussed in the previous sections. As depicted in Figure 1.12, the photosensitizer first absorbs light and becomes excited (i). The excited-state dye reduces an oxidant and forms the corresponding oxidized state (ii). The light absorber in the oxidized state returns to the ground state by accepting an electron from the valence band of the semiconductor (iii). The generated hole in the semiconductor is consumed by the water oxidation reaction on the surface, and O_2 is evolved. The DSP reactions were performed by combining the POMs with tris(1,10-phenanthroline) ruthenium(II) dye, and the cationic dye and anionic POMs strongly interacted. The O_2-evolution activity was strongly dependent on the cluster size and decreased in the order α-$[Mo_8O_{26}]^{4-} > [Mo_5S_2O_{23}]^{4-} > [Mo_6O_{19}]^{2-}$. This trend corresponds well to the number of Mo_5O_t (terminal oxygen) bonds: 14 in α-$[Mo_8O_{26}]^{4-}$, 10 in $[Mo_5S_2O_{23}]^{4-}$, and 6 in $[Mo_6O_{19}]^{2-}$. These results are reasonable because the Mo_5O_t bonds in POM photocatalysts are known to be the active sites for the oxidation reaction. The use of dye-sensitized systems enables the effect of cluster size to be investigated without interference from other physicochemical properties.

1.3.3 Highly Dispersed Active-Site Molybdenum Sulfide Nanoparticles for Proton Reduction Reaction

The importance of the active sites was demonstrated in Section 1.3.2. In a heterogeneous system, the number of active sites can be increased by well dispersing catalyst (or cocatalyst) nanoparticles because highly dispersed nanoparticles have a large specific surface area. To facilitate the H_2-evolution reaction, noble metals such as Pt, Pd, and Rh have been widely used. Molybdenum sulfides are potential candidates to replace these noble-metal H_2 evolution catalysts. Amorphous MoS_x has been reported to function as a highly active water-reduction catalyst with performance comparable to that of noble metals [81].

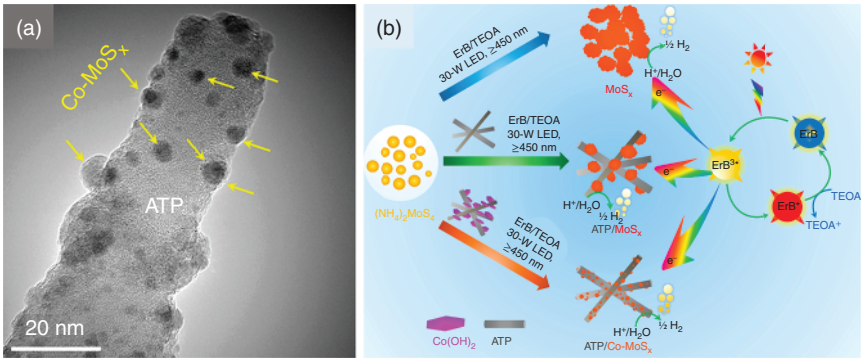

Figure 1.13 (a) HRTEM image of an ATP/Co-MoS_x catalyst. (b) Scheme of the in situ photochemical preparation of amorphous MoS_x, ATP/MoS_x, and ATP/Co-MoS_x and the photocatalytic H_2-evolution reaction. ErB: Erythrosine B photosensitizer, TEOA: triethanolamine electron donor. Source: Reproduced with permission from Liu et al. [82]; © 2018, American Chemical Society.

Amorphous and colloidal MoS_x have been applied to DSP H_2 production and have shown potential for both functioning a semiconductor and providing active sites [15, 82]. MoS_x is also known to be further activated by transition-metal doping to modulate its electronic properties, which can be carried out during in situ photodeposition [82]. The in situ growth of amorphous MoS_x, however, tends to result in its aggregation into particles as large as several hundred nanometers. To avoid aggregation, transition-metal-doped MoS_x was synthesized in situ using $Co(OH)_2$-modified attapulgite (ATP) nanofibers as starting materials. As a result, highly dispersed amorphous Co-doped MoS_x was successfully formed on ATP nanofibers (ATP/Co-MoS_x, Figure 1.13a) [82]. Notably, in situ growth without ATP or $Co(OH)_2$ resulted in micrometer-sized particles of MoS_x or ATP/MoS_x, respectively, and ATP, an insulator, served as a substrate. The photocatalytic H_2-evolution reaction was conducted in a mixed solution of Erythrosine B dye under visible light (Figure 1.13b). The activity of the ATP/Co-MoS_x was 67 and 10 times greater than that of the MoS_x particle catalyst and the ATP/MoS_x, respectively. Because the MoS_x catalysts function not only as active sites for H_2 evolution but also as an electron-conductive substrate in this system, highly dispersed MoS_x promotes electron transfer from the excited Erythrosine B dyes.

1.3.4 Improving the Solar Energy Conversion Efficiency by Suppressing Undesirable Backward Reactions

Introducing active sites for a catalytic reaction can accelerate not only the forward reactions but also undesirable backward reactions. In the case of the DSP half-reaction, the backward reaction is re-reduction or re-oxidation of a reversible electron donor, e.g. re-reduction of I_3^- in I_3^-/I^- redox system. Because such backward redox reactions are usually thermodynamically favored over the catalytic formation of H_2 or O_2, these reactions often dominate the efficiency of the

whole system. When a photocatalysis system evolves H_2 and O_2 simultaneously, the backward reaction of water formation from them should also be suppressed because a proton-reduction catalyst usually promotes the backward reaction. Overall water splitting is often achieved in a two-step excitation system: the so-called Z-scheme. In the Z-scheme process, two semiconductors catalyze H_2 and O_2 evolution, whereas a redox shuttle reagent mediates electron transfer between the two photocatalysts. Therefore, suppressing the undesirable reactions is paramount for improving the solar energy conversion efficiency.

A straightforward method to suppress backward reactions involving more reducible or oxidizable products is physical separation of the products from the active sites for forward reactions [83]. In the case of Pt-loaded layered oxide semiconductors, Pt nanoparticles are intercalated into the layers of the oxide. Protons can reach the intercalated Pt, whereas I_3^- ions cannot because of their large size. Researchers have also confirmed that the intercalation of Pt catalysts inhibits H_2–O_2 recombination [84]. The backward reaction of I_3^- to I^- was also found to be inhibited by surface modification using poly(styrenesulfonate), which led to as much as a fivefold improvement of the H_2-evolution activity compared with that of the unmodified catalyst [85]. An amide-functionalized reduced graphene oxide (RGO) modified with Pt could function as a good building block for DSP H_2 evolution [86]. Because the functionalized amide groups strongly adsorb O_2 molecules as a result of orbital hybridization between an N 2*p* orbital of the amide group and an O 2p orbital of an O_2 molecule, the concentration of dissolved O_2 molecules in the reaction solution was decreased and the backward water formation reaction was suppressed on Pt.

Backward electron transfer events other than the redox reactions should also be considered as undesirable processes in the DSP cycle. Back electron transfer occurs at the origin of injected electrons in the conduction band. The electrons in the semiconductor can drive the reduction reaction of the photosensitizers in the oxidized state. Nishioka et al. achieved inhibition of back electron transfer by modifying the semiconductor surface with Al_2O_3 [87]. The effect of Al_2O_3 was investigated by transient absorption measurement, which revealed that the suppression arises from physical separation of the adsorbed dye from the semiconductor. Notably, injection of the excited electron into the semiconductor was hardly affected by the Al_2O_3 modification, whereas the back electron transfer process was clearly inhibited.

Oshima et al. combined these two physical separation processes for suppressing the backward reaction with an electron mediator and the back electron transfer to develop a dye-sensitized photocatalyst [84]. The catalyst comprised calcium niobate nanosheets intercalated with a Pt cocatalyst for H_2 evolution and further modified with an Al_2O_3 layer. The Z-scheme water-splitting reaction was performed using a Ru(II) trisdiimine complex sensitizer combined with a PtO_x/H–Cs–WO_3 water-oxidation photocatalyst (Figure 1.14). The photocatalyst system achieved an AQY of 2.4% for water splitting under visible-light irradiation, which is the highest AQY reported to date for a dye-sensitized overall water-splitting system.

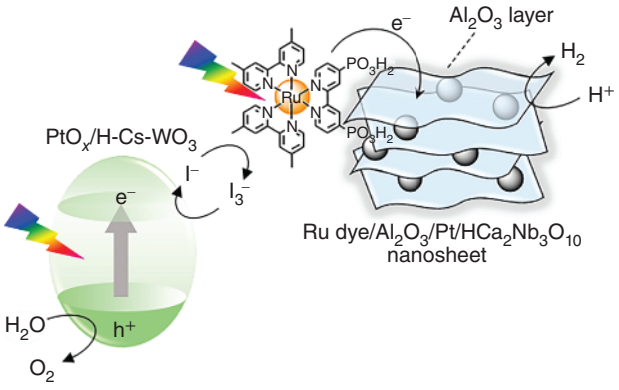

Figure 1.14 Schematic of Z-scheme water splitting using Ru dye-sensitized Al_2O_3/Pt/$HCa_2Nb_3O_{10}$ nanosheets and PtO_x/H–Cs–WO_3. Source: Reproduced with permission from Oshima et al. [84]; © 2020, American Chemical Society.

1.3.5 Immobilization of Dyes on a Reduced Graphene Oxide Surface Through Formation of Chemical Bonds

Graphene-based materials are among the most attractive conducting materials. Graphene has been used in electron-conductive devices because of its unusual properties, which include a high specific surface area, high intrinsic mobility, and high optical transmittance [88]. The oxidized form, graphene oxide (GO), is highly hydrophilic and can be suspended in an aqueous environment. The trade-off for hydrophilicity, however, is that GO lacks sufficiently high conductivity because of the disruption of the "graphitic" networks of graphene [89]. The electrical conductivity can be restored by reducing GO to form RGO. RGO possesses a substantial amount of O atoms in its structure (atomic C/O ratio: ~10), and its properties clearly differ from those of pristine graphene [89]. Because of its properties, RGO can be well dispersed in aqueous solutions and exhibits moderate electrical conductivity. Because these properties are beneficial for the water-splitting reaction, RGO has been applied as a conductor building block for H_2-evolution DSP systems [90, 91].

The organic texture of RGO enables dye molecules to be immobilized on their surface through the formation of chemical bonds. A silicon phthalocyanine dye (**SiPc**) was stabilized on N-doped RGO (N-RGO) by forming O–Si–O bonds with the O atom of a phenol moiety as a result of treating N-RGO with *N*-methyl glycine and 4-formylphenol [90]. The formation of a chemical bond between a dye and a semiconductor improves the electron-injection efficiency and the stability between them. An **SiPc**- and Pt-comodified N-RGO hybrid photocatalyst showed stable H_2-evolution activity for more than 30 hours. Similar chemical bond formation between the RGO and dye was performed in an RGO-**N749** system [91]. **N749** dyes were combined with RGO through an amine-terminated six-armed polyethylene glycol moiety. Because of the chemical bonding, the hybrid material showed high stability for 30 hours of photocatalytic reaction, similar to the stability of the **SiPc**–RGO system. The H_2 evolution activity of the hybrid material, however, was

poor: less than 1% of the AQY for the H_2-evolution half-reaction under visible-light irradiation. The moderate photocatalytic activities likely arose from the difficulty of engineering energy levels as a result of the loss of the semiconductive character.

1.3.6 Metal Phospho-Sulfides and -Selenides as Electron-Conducting and Proton-Adsorbing Materials

Metal phosphide nanomaterials have recently attracted attention as electrocatalysts and photocatalysts. A bimetallic phosphide can generate H_2 and O_2 in different DSP systems (i.e. Eosin-Y sensitization for H_2 and $[Ru(bpy)_3]^{2+}$ sensitization for O_2 evolution) [92]. An important role of phosphorus is the attraction of the proton to the surface of a metal phosphide. Increasing the ratio of phosphorus in a metal phosphide increases its electrochemical H_2-evolution activity [93]. For use in semiconductor photocatalysis, metal phospho-sulfides and -selenides (MPX_3, M = metal, X = S, Se) showing semiconducting behavior with 1.2–3.4 eV bandgaps have been developed [94]. As the metal in MPX_3, divalent cations (V^{2+}, Mn^{2+}, Fe^{2+}, Co^{2+}, Ni^{2+}, Zn^{2+}, Cd^{2+}, Sn^{2+}, or Hg^{2+}) for the M^{2+} system ($M^{2+}PX_3$) or monovalent cations (Ag^+ or Cu^+) and trivalent cations (Cr^{3+}, V^{3+}, Al^{3+}, Ga^{3+}, In^{3+}, or Bi^{3+}) for the $M^{1+} + M^{3+}$ system ($M^{1+}_{0.5}M^{3+}_{0.5}PX_3$) have been reported [95]. Ten types of MPX_3 (M = Ag^+, Ni^{2+}, Fe^{2+}, Cd^{2+}, Mn^{2+}, Zn^{2+}, In^{3+}; X = S, Se) were synthesized and used in DSP systems with Eosin-Y as a dye sensitizer. The activities were strongly dependent on the metal cation. The investigation led to three main findings: the activity was enhanced with (1) decreasing energy of the conduction-band minimum, (2) decreasing free energy for the adsorption of protons, and (3) decreasing P—P bond length. Trend (1) is opposite that of the Ru(II) complex–niobate-based nanosheet hybrid system mentioned in the introduction of this section [62], likely reflecting the difference in the reactions. In the case of Ru(II) complexes, they are chemically adsorbed onto the nanosheets and the electron injection occurs quickly from the adsorbed sensitizer upon photoexcitation. However, in the case of MPX_3, the H_2-evolution reaction was conducted in a physical mixture of MPX_3 and Eosin-Y. In this case, dye-to-MPX_3 electron injection appears to be slow compared with that in the hybridized system. Point (2), enhanced activity with decreasing free energy for the adsorption of protons, is well consistent with the metal phosphide catalyst, as previously described. Point (3), related to the P—P bond length, influences the electron density at each P center, which is the active site for the H_2-evolution reaction [94]. The antibonding levels of the P—P bond constitute the conduction band with the *s* and *p* orbitals of the metal. An increase in the P—P bond length leads to a decrease in the electron density at the P center, weakening the orbital overlap with the *s* and *p* orbitals of the metal (i.e. increasing the potential of the conduction band minimum). As a result, the activity is reduced.

1.3.7 Effects of Dye Adsorption for the Electronic State of the Semiconductor

As described in Section 1.2, strong electronic interaction between a semiconductor and the adsorbed sensitizer will affect the absorption of the dye and is the origin of

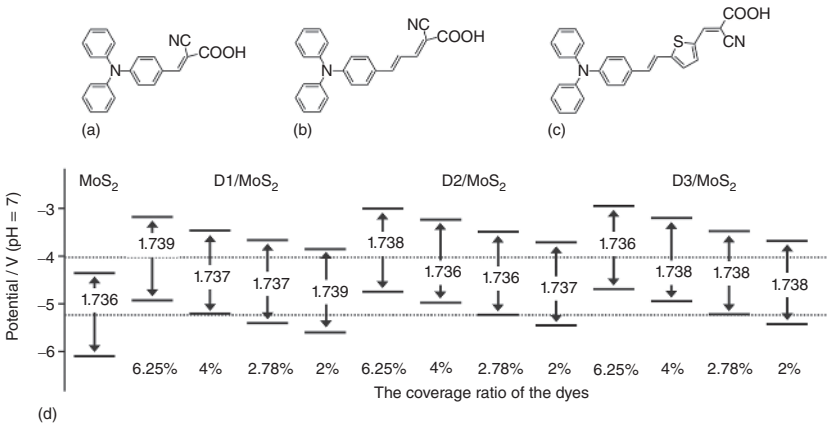

Figure 1.15 Molecular structures of (a) **D1**, (b) **D2**, and (c) **D3**. (d) Calculated band potentials of MoS_2 and dye-adsorbed MoS_2 with different dye coverage ratios. Source: Reproduced with permission from Pan et al. [96]; © 2020, American Chemical Society.

the very fast excited-electron injection that occurs on a timescale of femtoseconds to picoseconds. Such strong coupling should also influence the electronic state of the semiconductor. Because the bulk properties of the semiconductor would not be influenced even by the very strong interaction, a two-dimensional material is suitable to investigate the effect of an adsorbed dye on the semiconductor properties. By employing a monolayer of molybdenum sulfide as the semiconductor and three triphenylamine-based dyes, Pan et al. studied the electronic interaction between the two components through computational modeling and calculations (Figure 1.15a–c) [96]. The band edges of MoS_2 were shifted negatively by dye adsorption, and the degree of the negative shift increased with increasing intrinsic dipoles of the sensitizer (Figure 1.15d). These negative shifts could also be controlled by the surface coverage of the molecular dye. The band-edge potentials of monolayer MoS_2, which were originally not suitable for the water-splitting reaction, were found to straddle the water reduction/oxidation potentials upon dye adsorption. The calculation results suggested that dye adsorption varies the band potential of MoS_2, at least on the surface, even for bulky MoS_2.

1.4 Dye-sensitized Photocatalysts in Electrochemical Systems

Dye-sensitized photocatalysts have been applied in a photoelectrochemical cell that produces H_2 and O_2 from water [97–101]. There are two types of photoelectrochemical water-splitting cells: a water-oxidation photoanode [97–99] and a water-reduction photocathode [100, 101]. For a photoanode, dye-sensitized *n*-type semiconductors (e.g. TiO_2) are used as an electron-conductive substrate (Figure 1.16a). The injected electrons in TiO_2 migrate to the counter electrode through an external circuit because of upward band bending formed at the semiconductor–solution interface and are finally consumed to reduce water to H_2.

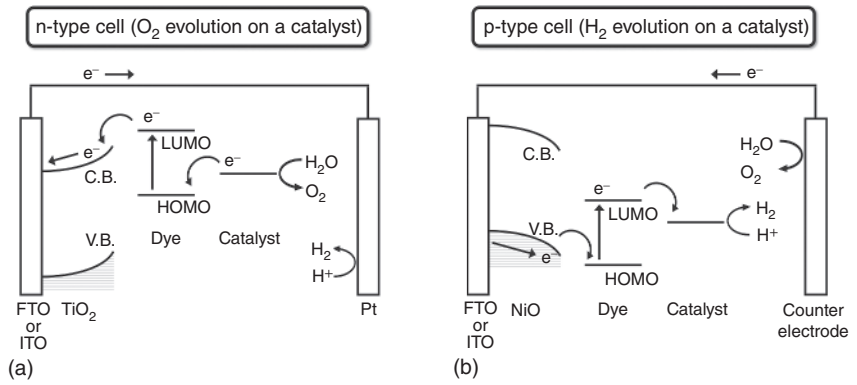

Figure 1.16 Schematic of water-splitting dye-sensitized (a) n-type and (b) p-type cells.

The oxidized sensitizer must accept an electron from water for O_2 evolution, hence necessitating a catalyst. For a photocathode, by contrast, dye-sensitized *p*-type semiconductors (e.g. NiO) are used (Figure 1.16b). The excited electrons in the dye are transferred to the catalyst and expended to reduce a proton for H_2 evolution. The oxidized dye receives an electron from the *p*-type semiconductor and returns to the ground state. The electrons are generated through the water oxidation reaction on the counter electrode and are transported via the external circuit. These are typical dye-sensitized photoelectrochemical water-splitting cycles.

To promote the catalytic reactions on the photoelectrodes, two main strategies have been studied. One strategy is to incorporate a catalyst into the photosensitizer [97, 100]. Another is to hybridize the dye and a molecular catalyst [99, 101]. In the case of catalyst–dye integration, cocatalysts for water splitting (e.g. IrO_x for O_2 evolution, Pt and Pd for H_2 evolution) are often selected as the catalyst. A colloidal IrO_2 water oxidation catalyst was adsorbed onto a photosensitizer with a dimethylmalonyl-anchoring moiety, which is not used for adsorbing dye molecules onto TiO_2 electrodes [97]. Although this photoanode functioned as a water-oxidation photoelectrode, the reaction efficiency was not sufficient because the forward electron transfer from IrO_2 into the photosensitizer was much slower than the undesirable electron transfers (i.e. electron transfers from TiO_2 into the oxidized dye and from the excited dye into IrO_2).

Pt and Pd catalysts incorporated into photosensitizers have been developed as water-reduction photocathodes [100]. Pt and Pd metal centers were integrated by forming a chemical bond with a ligand of the sensitizer. Although the integration of a metal center and dye improved the photoelectrochemical H_2-evolution activity compared with that of a system with separated dyes and catalysts, it required a large applied electrochemical bias for efficient catalytic reaction. This requirement is due to the undesirable electron transfer processes, similar to the case of the IrO_2 water-oxidation photoanode.

To avoid the unwanted electron transfer, physical separation between an electron- and a hole- collector is one of the effective approaches. The LBL assembly technique has been widely used, as described in Section 1.2.6 [99]. The LBL photoanodes

contained a conductive indium tin oxide electrode (semiconductor), methyl viologen (electron acceptor), Ru(II) trisdiimine complex (light absorber), Fe(II) bisterpyridine complex (electron donor), and Ru(II) water oxidation catalyst (Figure 1.17). The physical separation clearly inhibited the undesirable electron transfer events. Furthermore, the insertion of the electron acceptor between the electrode and the light absorber promoted the forward electron injection. The maximum value of incident photon-to-current efficiency reached 2.3% at 440 nm for the water-oxidation reaction, indicating that the physical separation strategy worked on a water-oxidation photoanode system. In addition, a noticeable feature of the method is its usability for both the photoanode and the photocathode depending on the structural design, even if the same light absorber is employed [102].

Notably, dye-sensitized photocathodes have been used in CO_2 reduction systems based on LBL assembly [103] and a highly stable metal-complex polymer [104]. The Ru-complex polymer system achieved CO_2 reduction in water and simultaneous O_2 evolution without any applied electrical bias [104]. This remarkable accomplishment demonstrates the promise of photoelectrosynthesis for advancing solar energy conversion.

1.5 Conclusion

We here reviewed recent progress in dye-sensitized photocatalysis, with focus on the building blocks, which are light absorbers and semiconductor materials. Important factors and strategies to improve the photocatalytic performance were discussed for each building block. For the molecular design of light absorbers, there are two significant trade-off relationships: Narrowing the HOMO–LUMO gap for longer-wavelength absorption adversely affects the electron transfer and redox processes because the driving force for these reactions is diminished, whereas strengthening the dye adsorption to improve stability can adversely affect the energy conversion efficiency because the backward electron transfer may be also accelerated. These difficult problems can be remedied by the following strategies. To intensify the light absorption, the incorporation of a chemical unit with a large molar extinction coefficient into the light absorber or forming multiple layers of light absorbers is effective. To attain robust adsorption, the important point is not reinforcement of the bonding but coordination with multidentate ligands. For the semiconductor component, we focused on new materials as potential alternatives to the standard material, TiO_2. Numerous new electron-conductive materials applicable to dye-sensitized H_2 evolution have been reported. COFs and metal–phospho-sulfides are promising materials for the DSP system. Methods of promoting the forward reactions and suppressing the backward reactions were discussed with a focus on the active sites. In the last section, dye-sensitized photoelectrochemical cells were introduced as a promising technology for solar energy conversion applications.

As previously described, because numerous factors strongly influence the energy conversion efficiency of DSP systems, improving the systems is not simple. Conversely, numerous factors influence the efficiency, suggesting that dramatic

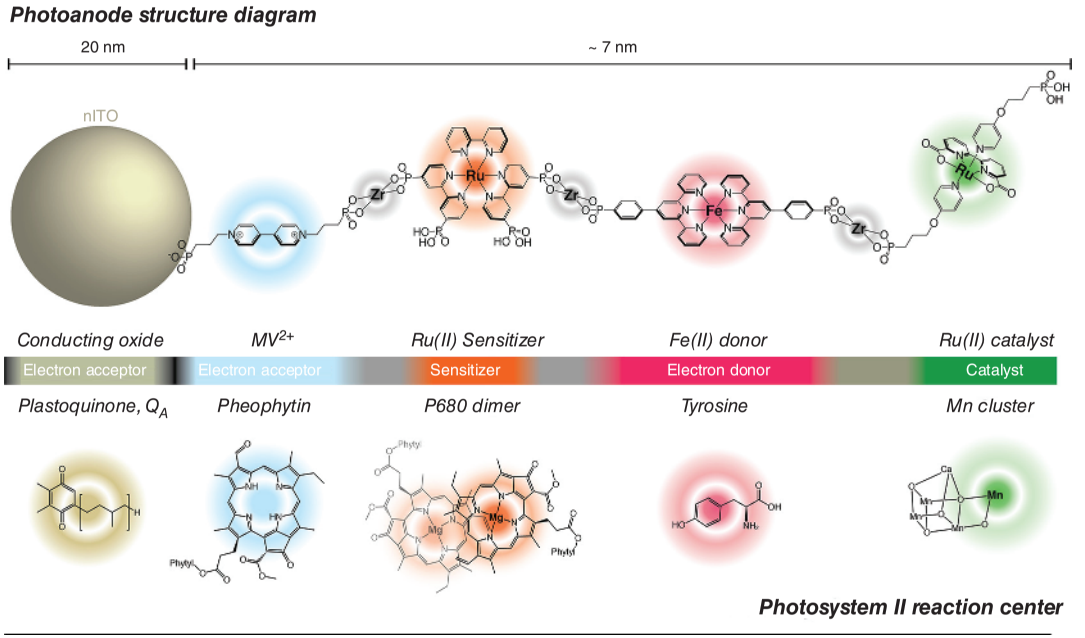

Figure 1.17 Structure of the molecular assembly of the four-molecular layer-by-layer photoanode and a diagram showing the key functional components of Photosystem II. Source: Reproduced with permission from Wang et al. [99]; © 2019, American Chemical Society.

improvements in DSP systems can be reasonably expected when many factors are understood and controlled. Such improvements require in-depth, detailed studies; for example, a kinetic study can reveal bottlenecks in a DSP system. Whereas kinetic studies have been extensively conducted in the DSSC field, the literature contains few detailed reports related to DSP systems. This dearth of information is attributable to the difficulty associated with using spectroscopic measurements to characterize DSP systems, a consequence of the reaction conditions, which typically involve a suspension. Powder suspension systems are basically not suitable for spectroscopic measurement. With improvements in the measurement techniques and analysis methods, however, some kinetic studies have been reported [105–107]. In the future, additional efforts should be devoted to understanding the reaction mechanisms in the dye-sensitized photocatalysis field.

References

1 Gerischer, H. (1972). Electrochemical techniques for the study of photosensitization. *Photochem. Photobiol.* 16: 243–260.

2 Borgarello, E., Kiwi, J., Pelizzettit, E. et al. (1981). Photochemical cleavage of water by photocatalysis. *Nature* 289: 158–160.

3 Reginato, G., Zani, L., Calamante, M. et al. (2020). Dye-sensitized heterogeneous photocatalysts for green redox reactions. *Eur. J. Inorg. Chem.* 2020: 899–917.

4 Brennaman, M.K., Dillon, R.J., Alibabaei, L. et al. (2016). Finding the way to solar fuels with dye-sensitized photoelectrosynthesis cells. *J. Am. Chem. Soc.* 138: 13085–13102.

5 Willkomm, J., Orchard, K.L., Reynal, A. et al. (2016). Dye-sensitised semiconductors modified with molecular catalysts for light-driven H_2 production. *Chem. Soc. Rev.* 45: 9–23.

6 Matsumura, M., Nomura, Y., and Tsubomura, H. (1977). Dye-sensitization on the photocurrent at zinc oxide electrode in aqueous electrolyte solution. *Bull. Chem. Soc. Jpn.* 50: 2533–2537.

7 O'Regan, B. and Grätzel, M. (1991). A low-cost, high-efficiency solar cell based on dye-sensitized colloidal TiO_2 films. *Nature* 353: 737–740.

8 Amadelli, R., Argazzi, R., Bignozzi, C.A., and Scandola, F. (1990). Design of antenna-sensitizer polynuclear complexes. Sensitization of titanium dioxide with $[Ru(bpy)_2(CN)_2]_2Ru(bpy(COO)_2)_2^{2-}$. *J. Am. Chem. Soc.* 112: 7099–7103.

9 Nazeeruddin, M.K., Kay, A., Rodicio, I. et al. (1993). Conversion of light to electricity by *cis*-X_2bis(2,2′-bipyridyl-4,4′-dicarboxylate)ruthenium(II) charge-transfer sensitizers (X=Cl^-, Br^-, I^-, CN^-, and SCN^-) on nanocrystalline TiO_2 electrodes. *J. Am. Chem. Soc.* 115: 6382–6390.

10 Nazeeruddin, M.K., Zakeeruddin, S.M., Humphry-Baker, R. et al. (1999). Acid-base equilibria of (2,2′-bipyridyl-4,4′-dicarboxylic acid)ruthenium(II) complexes and the effect of protonation on charge-transfer sensitization of nanocrystalline titania. *Inorg. Chem.* 38: 6298–6305.

11 Nazeeruddin, M.K., Splivallo, R., Liska, P. et al. (2003). A swift dye uptake procedure for dye sensitized solar cells. *Chem. Commun.* 12: 1456–1457.

12 Zhang, X., Veikko, U., Mao, J. et al. (2012). Visible-light-induced photocatalytic hydrogen production over binuclear Ru^{II}-bipyridyl dye-sensitized TiO_2 without noble metal loading. *Chem. Eur. J.* 18: 12103–12111.

13 Swetha, T., Mondal, I., Bhanuprakash, K. et al. (2015). First study on phosphonite-coordinated ruthenium sensitizers for efficient photocatalytic hydrogen evolution. *ACS Appl. Mater. Interfaces* 7: 19635–19642.

14 Wang, J., Zheng, Y., Peng, T. et al. (2017). Asymmetric zinc porphyrin derivative-sensitized graphitic carbon nitride for efficient visible-light-driven H_2 production. *ACS Sustain. Chem. Eng.* 5: 7549–7556.

15 Yuan, Y.J., Yu, Z.T., Liu, X.J. et al. (2014). Hydrogen photogeneration promoted by efficient electron transfer from iridium sensitizers to colloidal MoS_2 catalysts. *Sci. Rep.* 4: 4045.

16 Hirata, N., Lagref, J.J., Palomares, E.J. et al. (2004). Supramolecular control of charge-transfer dynamics on dye-sensitized nanocrystalline TiO_2 films. *Chem. Eur. J.* 10: 595–602.

17 Jayaweera, P.M., Kumarasinghe, A.R., and Tennakone, K. (1999). Nano-porous TiO_2 photovoltaic cells sensitized with metallochromic triphenylmethane dyes: [n-TiO_2/triphenylmethane dye/p-I^-/I_3^- (or CuI)]. *J. Photochem. Photobiol. A Chem.* 126: 111–115.

18 Kitamura, T., Ikeda, M., Shigaki, K. et al. (2004). Phenyl-conjugated oligoene sensitizers for TiO_2 solar cells. *Chem. Mater.* 16: 1806–1812.

19 Hagfeldt, A., Boschloo, G., Sun, L. et al. (2010). Dye-sensitized solar cells. *Chem. Rev.* 110: 6595–6663.

20 Mahmood, A. (2016). Triphenylamine based dyes for dye sensitized solar cells: a review. *Sol. Energy* 123: 127–144.

21 Ding, H., Chu, Y., Xu, M. et al. (2020). Effect of π-bridge groups based on indeno[1,2-*b*] thiophene D-A-π-A sensitizers on the performance of dye-sensitized solar cells and photocatalytic hydrogen evolution. *J. Mater. Chem. C* 8: 14864–14872.

22 Bartolini, M., Gombac, V., Sinicropi, A. et al. (2020). Tuning the properties of benzothiadiazole dyes for efficient visible light-driven photocatalytic H_2 production under different conditions. *ACS Appl. Energy Mater.* 3: 8912–8928.

23 Celil Yüzer, A., Genc, E., Harputlu, E. et al. (2020). Subphthalocyanine-sensitized TiO_2 photocatalyst for photoelectrochemical and photocatalytic hydrogen evolution. *Dalt. Trans.* 49: 12550–12554.

24 Abe, R., Shinmei, K., Koumura, N. et al. (2013). Visible-light-induced water splitting based on two-step photoexcitation between dye-sensitized layered niobate and tungsten oxide photocatalysts in the presence of a triiodide/iodide shuttle redox mediator. *J. Am. Chem. Soc.* 135: 16872–16884.

25 Yu, F., Wang, Z., Zhang, S. et al. (2018). N-annulated perylene-based organic dyes sensitized graphitic carbon nitride to form an amide bond for efficient photocatalytic hydrogen production under visible-light irradiation. *Appl. Catal. B Environ.* 237: 32–42.

26 Huang, J.F., Liu, J.M., Xiao, L.M. et al. (2019). Facile synthesis of porous hybrid materials based on Calix-3 dye and TiO_2 for high photocatalytic water splitting performance with excellent stability. *J. Mater. Chem. A* 7: 2993–2999.

27 Tiwari, A., Duvva, N., Rao, V.N. et al. (2019). Tetrathiafulvalene scaffold-based sensitizer on hierarchical porous TiO_2: efficient light-harvesting material for hydrogen production. *J. Phys. Chem. C* 123: 70–81.

28 Nazeeruddin, M.K., Péchy, P., Renouard, T. et al. (2001). Engineering of efficient panchromatic sensitizers for nanocrystalline TiO_2-based solar cells. *J. Am. Chem. Soc.* 123: 1613–1624.

29 Kinoshita, T., Dy, J.T., Uchida, S. et al. (2013). Wideband dye-sensitized solar cells employing a phosphine-coordinated ruthenium sensitizer. *Nat. Photonics* 7: 535–539.

30 Lin, Y.-D., Ke, B.-Y., Chang, Y.J. et al. (2015). Pyridomethene-BF_2 complex/phenothiazine hybrid sensitizer with high molar extinction coefficient for efficient, sensitized solar cells. *J. Mater. Chem. A* 3: 16831–16842.

31 Zhang, L. and Cole, J.M. (2017). Dye aggregation in dye-sensitized solar cells. *J. Mater. Chem. A* 5: 19541–19559.

32 Ning, Z., Zhang, Q., Wu, W. et al. (2008). Starburst triarylamine based dyes for efficient dye-sensitized solar cells. *J. Org. Chem.* 73: 3791–3797.

33 Huang, Z.-S., Meier, H., and Cao, D. (2016). Phenothiazine-based dyes for efficient dye-sensitized solar cells. *J. Mater. Chem. C* 4: 2404–2426.

34 Tian, H., Yang, X., Chen, R. et al. (2007). Phenothiazine derivatives for efficient organic dye-sensitized solar cells. *Chem. Commun.* 3741–3743.

35 Loudet, A. and Burgess, K. (2007). BODIPY dyes and their derivatives: Syntheses and spectroscopic properties. *Chem. Rev.* 107: 4891–4932.

36 Erten-Ela, S., Ueno, Y., Asaba, T., and Kubo, Y. (2017). Synthesis of a dibenzo-BODIPY-incorporating phenothiazine dye as a panchromatic sensitizer for dye-sensitized solar cells. *New J. Chem.* 41: 10367–10375.

37 Suryani, O., Higashino, Y., Sato, H., and Kubo, Y. (2019). Visible-to-near-infrared light-driven photocatalytic hydrogen production using dibenzo-bodipy and phenothiazine conjugate as organic photosensitizer. *ACS Appl. Energy Mater.* 2: 448–458.

38 Hara, K., Kurashige, M., Dan-Oh, Y. et al. (2003). Design of new coumarin dyes having thiophene moieties for highly efficient organic-dye-sensitized solar cells. *New J. Chem.* 27: 783–785.

39 Hagberg, D.P., Edvinsson, T., Marinado, T. et al. (2006). A novel organic chromophore for dye-sensitized nanostructured solar cells. *Chem. Commun.* 2245–2247.

40 Hagberg, D.P., Jiang, X., Gabrielsson, E. et al. (2009). Symmetric and unsymmetric donor functionalization. comparing structural and spectral benefits of chromophores for dye-sensitized solar cells. *J. Mater. Chem.* 19: 7232–7238.

41 Lim, K., Kim, C., Song, J. et al. (2011). Enhancing the performance of organic dye-sensitized solar cells via a slight structure modification. *J. Phys. Chem. C* 115: 22640–22646.

42 Li, R., Liu, J., Cai, N. et al. (2010). Synchronously reduced surface states, charge recombination, and light absorption length for high-performance organic dye-sensitized solar cells. *J. Phys. Chem. B* 114: 4461–4464.

43 Pei, K., Wu, Y., Islam, A. et al. (2013). Constructing high-efficiency D-A-π-A-featured solar cell sensitizers: A promising building block of 2,3-diphenylquinoxaline for antiaggregation and photostability. *ACS Appl. Mater. Interfaces* 5: 4986–4995.

44 Gabrielsson, E., Ellis, H., Feldt, S. et al. (2013). Convergent/divergent synthesis of a linker-varied series of dyes for dye-sensitized solar cells based on the D35 donor. *Adv. Energy Mater.* 3: 1647–1656.

45 Wu, Y. and Zhu, W. (2013). Organic sensitizers from D–π–A to D–A–π–A: Effect of the internal electron-withdrawing units on molecular absorption, energy levels and photovoltaic performances. *Chem. Soc. Rev.* 42: 2039–2058.

46 Wu, Y., Marszalek, M., Zakeeruddin, S.M. et al. (2012). High-conversion-efficiency organic dye-sensitized solar cells: Molecular engineering on D-A-π-A featured organic indoline dyes. *Energy Environ. Sci.* 5: 8261–8272.

47 Shen, Z., Xu, B., Liu, P. et al. (2017). High performance solid-state dye-sensitized solar cells based on organic blue-colored dyes. *J. Mater. Chem. A* 5: 1242–1247.

48 Watanabe, M., Hagiwara, H., Ogata, Y. et al. (2015). Impact of alkoxy chain length on carbazole-based, visible light-driven, dye sensitized photocatalytic hydrogen production. *J. Mater. Chem. A* 3: 21713–21721.

49 Manfredi, N., Cecconi, B., Calabrese, V. et al. (2016). Dye-sensitized photocatalytic hydrogen production: distinct activity in a glucose derivative of a phenothiazine dye. *Chem. Commun.* 52: 6977–6980.

50 Ishizaki, R., Fukino, R., Matsuzaki, H., and Katoh, R. (2017). Effect of adsorbed water molecules on light harvesting and electron injection processes in dye-sensitized nanocrystalline TiO_2 films. *J. Phys. Chem. C* 121: 16266–16274.

51 Asbury, J.B., Hao, E., Wang, Y. et al. (2001). Ultrafast electron transfer dynamics from molecular adsorbates to semiconductor nanocrystalline thin films. *J. Phys. Chem. B* 105: 4545–4557.

52 Park, H., Bae, E., Lee, J.J. et al. (2006). Effect of the anchoring group in Ru-bipyridyl sensitizers on the photoelectrochemical behavior of dye-sensitized TiO_2 electrodes: carboxylate versus phosphonate linkages. *J. Phys. Chem. B* 110: 8740–8749.

53 Manfredi, N., Cecconi, B., and Abbotto, A. (2014). Multi-branched multi-anchoring metal-free dyes for dye-sensitized solar cells. *European J. Org. Chem.* 7069–7086.

54 Tan, L., Liu, J., Li, S. et al. (2015). Dye-sensitized solar cells with improved performance using cone-Calix[4]arene based dyes. *ChemSusChem* 8: 280–287.

55 Chen, Y., Huang, J., Shen, M. et al. (2019). A porous hybrid material based on calixarene dye and TiO_2 demonstrating high and stable photocatalytic performance. *J. Mater. Chem. A* 7: 19852–19861.

56 Manfredi, N., Monai, M., Montini, T. et al. (2018). Dye-sensitized photocatalytic hydrogen generation: Efficiency enhancement by organic photosensitizer-coadsorbent intermolecular interaction. *ACS Energy Lett.* 3: 85–91.

57 George, L., Sappati, S., Ghosh, P., and Devi, R.N. (2018). Sensitizing with short conjugated molecules: Multimodal anchoring on ZnO nanoparticles for enhanced electron transfer characteristics, stability and H_2 evolution. *Catal. Today* 309: 89–97.

58 Lee, H., Kepley, L.J., Hong, H.G., and Mallouk, T.E. (1988). Inorganic analogues of Langmuir-Blodgett films: Adsorption of ordered zirconium 1,10-decanebisphosphonate multilayers on silicon surfaces. *J. Am. Chem. Soc.* 110: 618–620.

59 Hanson, K., Torelli, D.A., Vannucci, A.K. et al. (2012). Self-assembled bilayer films of ruthenium(II)/polypyridyl complexes through layer-by-layer deposition on nanostructured metal oxides. *Angew. Chem. Int. Ed.* 51: 12782–12785.

60 Yoshimura, N., Kobayashi, A., Yoshida, M., and Kato, M. (2020). Enhancement of photocatalytic activity for hydrogen production by surface modification of Pt-TiO_2 nanoparticles with a double layer of photosensitizers. *Chem. Eur. J.* 26: 16939–16946.

61 Huang, J.F., Lei, Y., Luo, T., and Liu, J.M. (2020). Photocatalytic H_2 production from water by metal-free dye-sensitized TiO_2 semiconductors: the role and development process of organic sensitizers. *ChemSusChem* 13: 5863–5895.

62 Maeda, K., Sahara, G., Eguchi, M., and Ishitani, O. (2015). Hybrids of a ruthenium(II) polypyridyl complex and a metal oxide nanosheet for dye-sensitized hydrogen evolution with visible light: effects of the energy structure on photocatalytic activity. *ACS Catal.* 5: 1700–1707.

63 Maeda, K., Eguchi, M., Youngblood, W.J., and Mallouk, T.E. (2008). Niobium oxide nanoscrolls as building blocks for dye-sensitized hydrogen production from water under visible light irradiation. *Chem. Mater.* 20: 6770–6778.

64 Han, L., Lv, Y., Li, B. et al. (2020). Enhancing H_2 evolution and molecular oxygen activation via dye sensitized $BiOBr_{0.9}I_{0.1}$ under visible light. *J. Colloid Interface Sci.* 580: 1–10.

65 Zhang, W. and Lu, G. (2016). The enhancement of electron transportation and photo-catalytic activity for hydrogen generation by introducing spin-polarized current into dye-sensitized photo-catalyst. *Catal. Sci. Technol.* 6: 7693–7697.

66 Kong, C., Han, xia, Y., Hou, jie, L., and Li, ying, Y. (2017). Gathered sensitizer on the surface of catalyst by sodium polyacrylate for highly efficient photocatalytic hydrogen evolution. *J. Photochem. Photobiol. A Chem.* 345: 92–97.

67 Tajima, T., Yamagami, M., Sagawa, R. et al. (2021). Dye-sensitized H_2 evolution from water facilitated by photoinduced electron transfer between molecules on the inside and the outside of a carbon nanotube. *J. Appl. Phys.* 129: 014303.

68 Wu, L., Tong, Y., Gu, L. et al. (2018). MOFs as an electron-transfer-bridge between a dye photosensitizer and a low cost Ni_2P co-catalyst for increased photocatalytic H_2 generation. *Sustain. Energy Fuels* 2: 2502–2506.

69 Liu, X., Zhao, L., Wang, H. et al. (2018). Visible-light-driven H_2 production and decomposition of 4-nitrophenol over nickel phosphides. *RSC Adv.* 8: 34259–34265.

70 Lei, Q., Long, X., Chen, H. et al. (2019). Facilitating charge transfer *via* magnetoresistance effect for high-efficiency photocatalytic hydrogen production. *Chem. Commun.* 55: 14478–14481.

71 Panagiotopoulos, A., Douvas, A.M., Argitis, P., and Coutsolelos, A.G. (2016). Porphyrin-sensitized evolution of hydrogen using Dawson and Keplerate polyoxometalate photocatalysts. *ChemSusChem* 9: 3213–3219.

72 Sun, Y., Sun, Y., Meng, X. et al. (2019). Eosin Y-sensitized partially oxidized Ti_3C_2 MXene for photocatalytic hydrogen evolution. *Catal. Sci. Technol.* 9: 310–315.

73 Wang, X., Chen, L., Chong, S.Y. et al. (2018). Sulfone-containing covalent organic frameworks for photocatalytic hydrogen evolution from water. *Nat. Chem.* 10: 1180–1189.

74 Wan, S., Gándara, F., Asano, A. et al. (2011). Covalent organic frameworks with high charge carrier mobility. *Chem. Mater.* 23: 4094–4097.

75 Sprick, R.S., Bonillo, B., Clowes, R. et al. (2016). Visible-light-driven hydrogen evolution using planarized conjugated polymer photocatalysts. *Angew. Chem. Int. Ed.* 55: 1792–1796.

76 Vyas, V.S., Haase, F., Stegbauer, L. et al. (2015). A tunable azine covalent organic framework platform for visible light-induced hydrogen generation. *Nat. Commun.* 6: 8508.

77 Walsh, J.J., Bond, A.M., Forster, R.J., and Keyes, T.E. (2016). Hybrid polyoxometalate materials for photo(electro-) chemical applications. *Coord. Chem. Rev.* 306: 217–234.

78 Tachikawa, T., Fujitsuka, M., and Majima, T. (2007). Mechanistic insight into the TiO_2 photocatalytic reactions: design of new photocatalysts. *J. Phys. Chem. C* 111: 5259–5275.

79 Hiskia, A., Mylonas, A., and Papaconstantinou, E. (2001). Comparison of the photoredox properties of polyoxometallates and semiconducting particles. *Chem. Soc. Rev.* 30: 62–69.

80 Gao, J., Cao, S., Tay, Q. et al. (2013). Molecule-based water-oxidation catalysts (WOCs): Cluster-size-dependent dye-sensitized polyoxometalates for visible-light-driven O_2 evolution. *Sci. Rep.* 3: 1853.

81 Merki, D., Fierro, S., Vrubel, H., and Hu, X. (2011). Amorphous molybdenum sulfide films as catalysts for electrochemical hydrogen production in water. *Chem. Sci.* 2: 1262–1267.

82 Liu, X., Xue, Y., Lei, Y. et al. (2018). Cobalt-activated amorphous MoS_x nanodots grown in situ on natural attapulgite nanofibers for efficient visible-light-driven dye-sensitized H_2 evolution. *ACS Appl. Nano Mater.* 1: 6493–6501.

83 Kim, Y.I., Atherton, S.J., Brigham, E.S., and Mallouk, T.E. (1993). Sensitized layered metal oxide semiconductor particles for photochemical

hydrogen evolution from nonsacrificial electron donors. *J. Phys. Chem.* 97: 11802–11810.

84 Oshima, T., Nishioka, S., Kikuchi, Y. et al. (2020). An artificial Z-scheme constructed from dye-sensitized metal oxide nanosheets for visible light-driven overall water splitting. *J. Am. Chem. Soc.* 142: 8412–8420.

85 Saupe, G.B., Mallouk, T.E., Kim, W., and Schmehl, R.H. (1997). Visible light photolysis of hydrogen iodide using sensitized layered metal oxide semiconductors: The role of surface chemical modification in controlling back electron transfer reactions. *J. Phys. Chem. B* 101: 2508–2513.

86 Zhang, X., Luo, D., Zhang, W. et al. (2018). Inhibition of hydrogen and oxygen recombination over amide–functionalized graphene and the enhancement of photocatalytic hydrogen generation in dye–sensitized AF–RGO/Pt photocatalyst dispersion. *Appl. Catal. B Environ.* 232: 371–383.

87 Nishioka, S., Oshima, T., Hirai, S. et al. (2021). Excited carrier dynamics in a dye-sensitized niobate nanosheet photocatalyst for visible-light hydrogen evolution. *ACS Catal.* 11: 659–669.

88 Zhu, Y., Murali, S., Cai, W. et al. (2010). Graphene and graphene oxide: synthesis, properties, and applications. *Adv. Mater.* 22: 3906–3924.

89 Park, S. and Ruoff, R.S. (2009). Chemical methods for the production of graphenes. *Nat. Nanotechnol.* 4: 217–224.

90 Huang, J., Wu, Y., Wang, D. et al. (2015). Silicon phthalocyanine covalently functionalized N-doped ultrasmall reduced graphene oxide decorated with Pt nanoparticles for hydrogen evolution from water. *ACS Appl. Mater. Interfaces* 7: 3732–3741.

91 Huang, J., Wang, D., Yue, Z. et al. (2015). Ruthenium dye N749 covalently functionalized reduced graphene oxide: a novel photocatalyst for visible light H_2 evolution. *J. Phys. Chem. C* 119: 27892–27899.

92 Li, S., Tan, J., Jiang, Z. et al. (2020). MOF-derived bimetallic Fe-Ni-P nanotubes with tunable compositions for dye-sensitized photocatalytic H_2 and O_2 production. *Chem. Eng. J.* 384: 123354.

93 Shi, Y. and Zhang, B. (2016). Recent advances in transition metal phosphide nanomaterials: synthesis and applications in hydrogen evolution reaction. *Chem. Soc. Rev.* 45: 1529–1541.

94 Susner, M.A., Chyasnavichyus, M., McGuire, M.A. et al. (2017). Metal thio- and selenophosphates as multifunctional van der Waals layered materials. *Adv. Mater.* 29: 1602852.

95 Barua, M., Ayyub, M.M., Vishnoi, P. et al. (2019). Photochemical HER activity of layered metal phospho-sulfides and -selenides. *J. Mater. Chem. A* 7: 22500–22506.

96 Pan, J., Shao, X., Xu, X. et al. (2020). Organic dye molecules sensitization-enhanced photocatalytic water-splitting activity of MoS_2 from first-principles calculations. *J. Phys. Chem. C* 124: 6580–6587.

97 Youngblood, J.W., Lee, S.H.A., Kobayashi, Y. et al. (2009). Photoassisted overall water splitting in a visible light-absorbing dye-sensitized photoelectrochemical cell. *J. Am. Chem. Soc.* 131: 926–927.

98 Xu, P., Huang, T., Huang, J. et al. (2018). Dye-sensitized photoelectrochemical water oxidation through a buried junction. *Proc. Natl. Acad. Sci. U. S. A.* 115: 6946–6951.

99 Wang, D., Sampaio, R.N., Troian-Gautier, L. et al. (2019). Molecular photoelectrode for water oxidation inspired by photosystem II. *J. Am. Chem. Soc.* 141: 7926–7933.

100 Põldme, N., O'Reilly, L., Fletcher, I. et al. (2019). Photoelectrocatalytic H_2 evolution from integrated photocatalysts adsorbed on NiO. *Chem. Sci.* 10: 99–112.

101 Lyu, S., Massin, J., Pavone, M. et al. (2019). H_2-evolving dye-sensitized photocathode based on a ruthenium-diacetylide/cobaloxime supramolecular assembly. *ACS Appl. Energy Mater.* 2: 4971–4980.

102 Farnum, B.H., Wee, K.R., and Meyer, T.J. (2016). Self-assembled molecular p/n junctions for applications in dye-sensitized solar energy conversion. *Nat. Chem.* 8: 845–852.

103 Wang, D., Wang, Y., Brady, M.D. et al. (2019). A donor-chromophore-catalyst assembly for solar CO_2 reduction. *Chem. Sci.* 10: 4436–4444.

104 Kamata, R., Kumagai, H., Yamazaki, Y. et al. (2021). Durable photoelectrochemical CO_2 reduction with water oxidation using a visible-light driven molecular photocathode. *J. Mater. Chem. A* 9: 1517–1529.

105 Zhang, H., Li, S., Lu, R., and Yu, A. (2015). Time-resolved study on xanthene dye-sensitized carbon nitride photocatalytic systems. *ACS Appl. Mater. Interfaces* 7: 21868–21874.

106 Ma, H., Ma, W., Chen, J.F. et al. (2018). Quantifying visible-light-induced electron transfer properties of single dye-sensitized ZnO entity for water splitting. *J. Am. Chem. Soc.* 140: 5272–5279.

107 Nishioka, S., Yamazaki, Y., Okazaki, M. et al. (2019). Defect density-dependent electron injection from excited-state Ru(II) tris-diimine complexes into defect-controlled oxide semiconductors. *J. Phys. Chem. C* 123: 28310–28318.